Multidimensional Modelling of Long-Offset Transient Electromagnetics Data Collected at the South Flank of Mount Merapi, Indonesia

Thomas Kalscheuer, Stefan L. Helwig, Bülent Tezkan and Michael Commer[1]

Abstract

LOTEM data from the south flank of Mount Merapi, Indonesia, are interpreted with one-dimensional inversions as well as two- and three-dimensional forward modelling. One-dimensional (1D) joint inversions of several components of the electromagnetic field with Occam's method reduce the number of equivalent models derived from inversions of single components. Our 1D results together with results from other geophysical measurements serve as the basic model for further multi-dimensional forward modelling . The final model depicts a layering that follows the topography of the strato volcano. In a depth range of 500 m to 1000 m there is a transition to a good conductor with resistivities below 10 Ωm. We developed the hypothesis of a fault-like structure below the southern flank at approximately 7 km distance from the summit. To the north of the fault the transition to the good conductor is lowered to a depth of 1000 m.

1. Introduction

The Long Offset Transient Electromagnetics (LOTEM) method covers a depth range between a few hundred metres and a few kilometres (Strack, 1992), where major volcanic structures can be expected and is therefore suitable for the investigation of volcanic structures.

As a part of the interdisciplinary MERAPI (Mechanism Evaluation, Risk Assessment, Prediction Improvement) project (Zschau et al., 1998) LOTEM measurements were carried out along a north-south profile with a length of 12 km at the south flank of Mount Merapi (Figure 1). During a field campaign in 2001 a grounded electric dipole transmitter was placed at the southern end of the profile. At 38 receiver stations to the north of the transmitter horizontal electric field components as well as the time derivatives of the horizontal and vertical components of the magnetic field were recorded.

A first LOTEM campaign (Müller et al., 2002) took place in 1998 when the transmitter was located in the northern part of the same profile and electromagnetic transient fields were measured both north and south of the transmitter. The southern stations of this first campaign showed effects which cannot be explained by a one-dimensional (1D) conductivity distribution.

The joint interpretation of the 1998 and 2001 data has two aims. First, there is a strong interest in discovering whether the layering is correlated with the topography as it has been observed close to the summit (Commer, 2003). Second, we try to explain the observed anomalous effects with a two-dimensional (2D) model. Our model assumptions are based on the LOTEM measurements as well as earlier results from other geophysical methods, e.g. NanoTEM (Koch, 2003), DC-geoelectrics (Friedel et al., 2000) and magnetotellurics (Müller, 2000).

2. 1D-inversions of the 2001 data

A first 1D interpretation of transient fields measured in 2001 was achieved with the Occam inversion method (Constable et al., 1987). Single components were inverted with the the first and second derivatives of the resistivity distribution

$$R_1 = \int \left(\frac{dm}{dz} \right)^2 dz \tag{1}$$

and

$$R_2 = \int \left(\frac{d^2 m}{dz^2} \right)^2 dz \tag{2}$$

as smoothness constraints.

The first derivative minimizes changes in the models and hence leads to a constant resistivity curve in depth ranges where there is no sensitivity of the data. Applying the second derivative a model is reckoned smooth if the model exhibits a constant increase or decline of resistivity values with depth. The smoothness condition is implemented into the cost function U using the method of Lagrange multipliers (Constable et al., 1987):

$$U = \left\| \partial \boldsymbol{m} \right\|^2 + \mu^{-1} \left[\left\| \boldsymbol{d} - \boldsymbol{F}[\boldsymbol{m}] \right\|_{\mathbf{W}}^2 \right] \tag{3}$$

[1]Institut für Geophysik und Meteorologie, Universität zu Köln, Albertus-Magnus-PLatz, D-50923 Köln

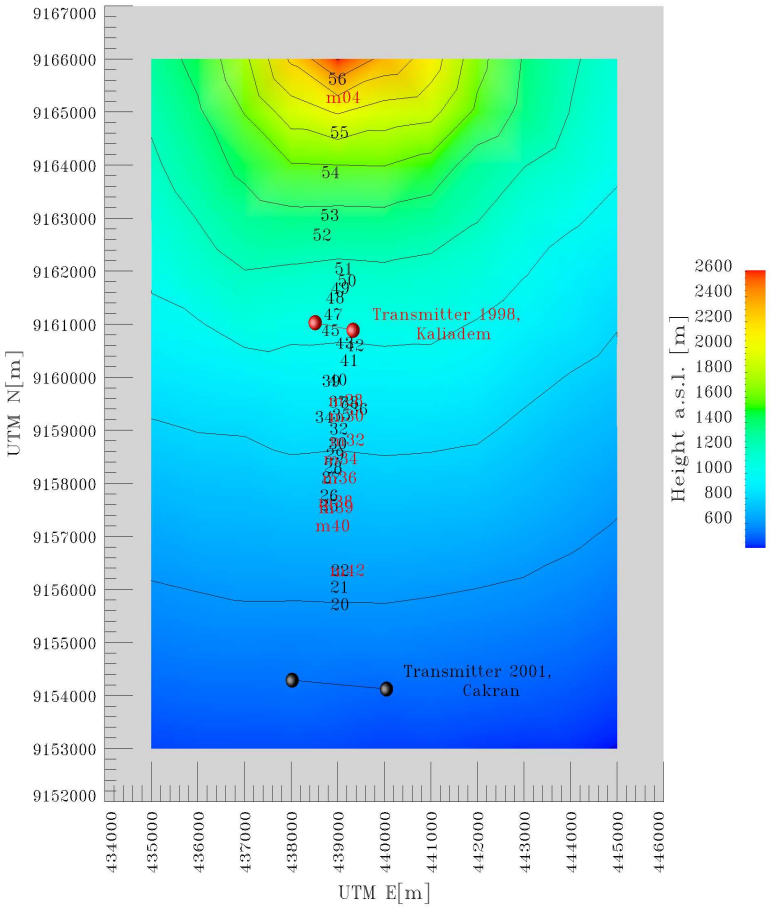

Figure 1: *Topographical map of the measurement area at the south flank of Mount Merapi. Transmitter and receiver positions used during the 1998 and 2001 field campaign are marked by red and black boxes, respectively.*

Here, $\partial \boldsymbol{m}$ designates the discrete version of R_1 where ∂ is a matrix derivative operator. $\left\|\boldsymbol{d} - \boldsymbol{F}[\boldsymbol{m}]\right\|^2_{\mathbf{W}}$ is the weighted sum of differences between the elements of the field data vector $\boldsymbol{d}$ and the forward data vector $\boldsymbol{F}[\boldsymbol{m}]$. Finally, the Lagrange factor μ can be described as a trade-off between data fit and model smoothness. After minimizing U with respect to $\boldsymbol{m}$ during the inversion, this factor is determined through a line search to minimize the data misfit $\left\|\boldsymbol{d} - \boldsymbol{F}[\boldsymbol{m}]\right\|_{\mathbf{W}}$ (Constable et al., 1987).

Local, near-surface anomalies immediately below a receiver site can shift measured LOTEM transients. In order to account for this shift the forward response is multiplied by a calibration factor CF. The calibration factor is another free parameter during the inversion (Hördt, 1989).

The depth at which the model curves for different smoothness constraints diverge can be used as an estimate of the maximum depth of investigation (Commer, 1999). As an example, the inversion result of the $\dot{B}_y$ component of station 28 is presented in Figure 2. At a depth of about 1500 m the two model curves show a diverging behaviour. There is also disagreement between the models for depths above 400 m. Because of the resistive environment, the diffusion time to a depth of 400 m for the resistivity distributions given in Figure 2 is smaller than the sampling rate of 1 ms at which the transient was recorded. Corresponding to Spies (1989), this means, that the resistivity distribution of these upper layers cannot be resolved from the data.

By joint inversion (Vozoff and Jupp, 1975) of several electromagnetic field components a model was sought that explains all of the considered components. The data sets of different field components are combined to one data vector $\boldsymbol{d}$. Equivalently, forward model responses of the different field components need to be arranged to one forward vector $\boldsymbol{F}[\boldsymbol{m}]$. Joint inversion can increase the number of important model parameters (Vozoff and Jupp, 1975). Hence joint inversions

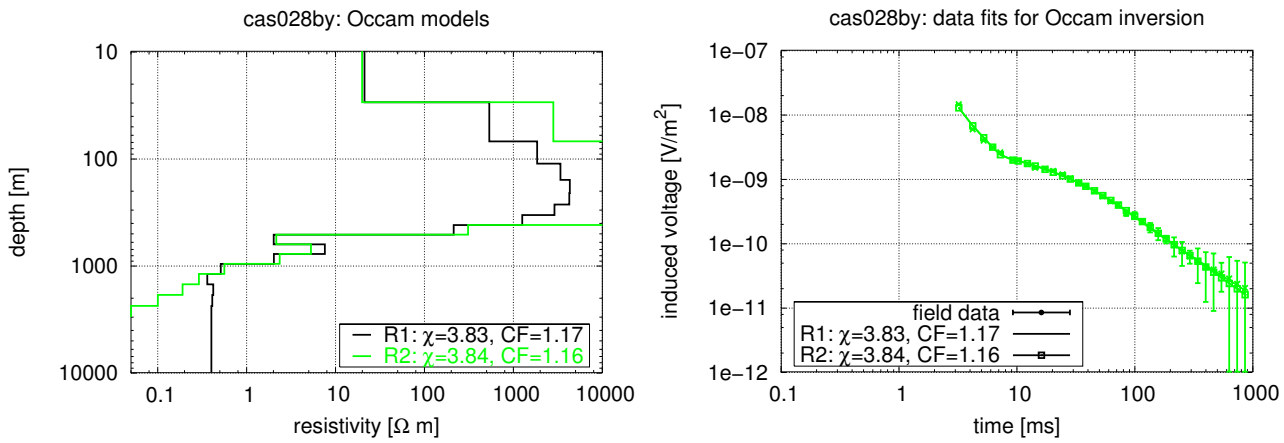

Figure 2: *1D-Models (left) for the $\dot{B}_y$ component of station 28 and data fits (χ-errors) yielded by smoothing with the first derivative (R_1) and second derivative (R_2), respectively (right).*

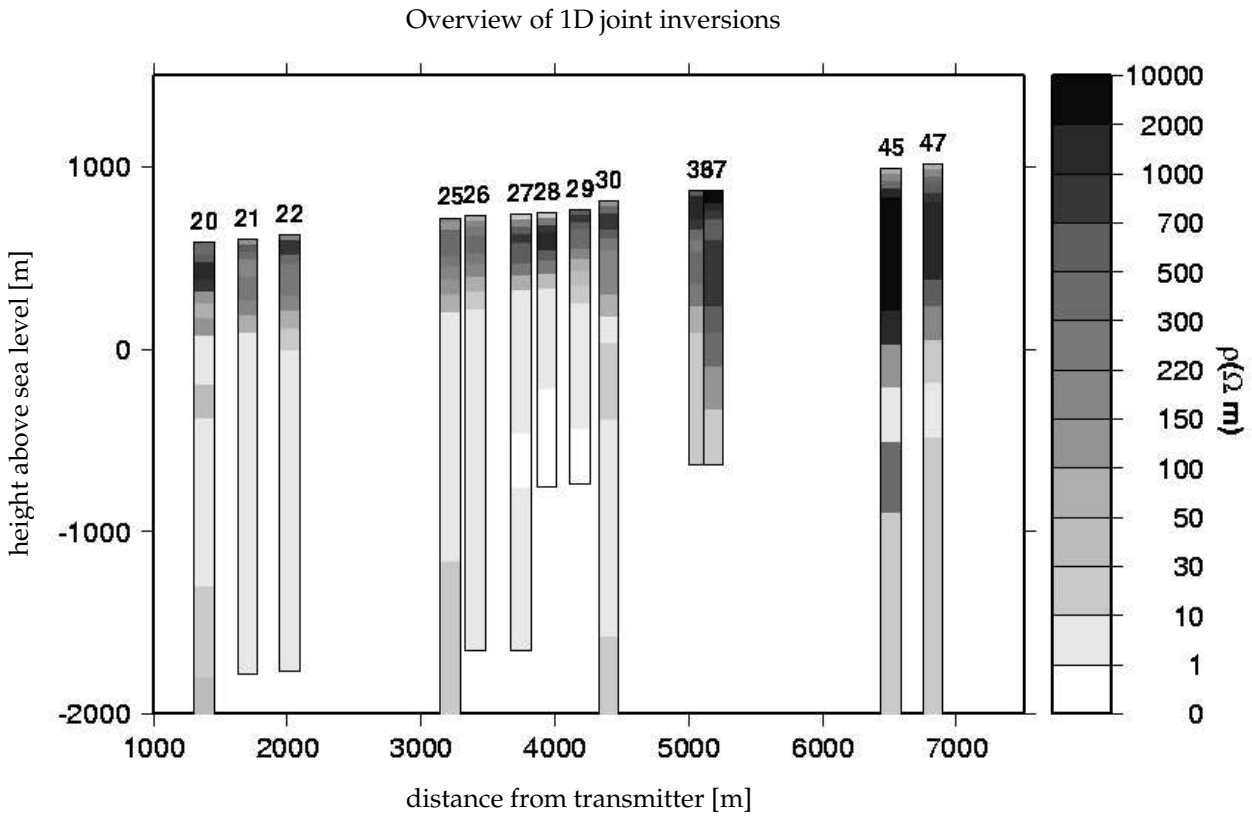

Figure 3: *1D-models derived by joint inversions. The maximum depth corresponds to the depth of investigation estimated by the comparison of the first and second derivatives as smoothness constraints.*

lead to a decrease of ambiguity, because the number of equivalent models which are derived from the inversions of single components is reduced (Vozoff and Jupp, 1975). Figure 3 shows the results of the joint inversions as a pseudo section along the profile with the top of each diagram following topography. The results of the 1D-joint inversions are conform to results of other geophysical methods. At a depth of 500 m to 1000 m a transition to a good conductor with resistivities below 10 Ωm is encountered. In general the resistivity distribution follows topography but the transition to the good conductor occurs at greater depth closer to the summit. The 1D-joint inversion results serve as a basis for further 2D and 3D forward modelling.

3. Multidimensional effects

Due to the position of the transmitter at the southern end of the profile in 2001 there is important supplementary information to the data collected in 1998. The $\dot{B}_z$-components of the 1998 stations located to the south of the corresponding transmitter position displayed double sign reversals, which cannot be caused by a 1D layering. Müller et al. (2002) accomplished a first qualitative explanation of the sign changes in the 1998 LOTEM data with an east-west striking block in a homogeneous halfspace. Although this simplified model explains the occurences of sign reversals it contradicts with the transition to a good conductor at a depth of 500 m to 1000 m as proposed by the 1D joint inversions of the 2001 LOTEM data (Figure 3).
The existence of an anomalous resistivity distribution on this part of the profile was confirmed by NanoTEM-measurements (Koch, 2003) and magnetotelluric measurements (Müller, 2000). An anomaly is also indicated by the results of the 1D-joint inversions of the 2001 LOTEM data (Figure 3) between station 30 and 36. There are further signs of multidimensional effects in the $\dot{B}_z$-components of the 2001 LOTEM data. Unfortunately, the data quality at these stations is rather bad due to strong noise effects which could not be filtered out. Although a multi-dimensional resistivity distribution is indicated by the data of stations 30 to 40, its exact shape cannot be reconstructed with the data set currently available.

4. 2D-forward modelling

For two-dimensional forward modelling the program `maxwell` written by Druskin and Knizhnerman (1988) was used. This code calculates an model forward response on a finite difference grid using a spectral Lanczos decomposition scheme.
A geological interpretation of our 1D-results of the 2001 data (Figure 3) suggests a fault located at a distance of 4700 m to 5200 m to the north of the transmitter. In the southern section a good conductor appears at a depth of 500 m. North of the assumed fault the good conductor appears at greater depths. In several steps we developed the 2D resistivity model given in Figure 4 which comprises these main features and explains many details of the 2001 data. In the following paragraphs we outline the main arguments leading to our final model.
The upper layers to a depth of a few hundred metres cannot be resolved by the LOTEM transients which were recorded in the field because of the high resistivities encountered and the recording interval of 1 ms to 1 s. However, an improvement of fit to amplitudes of our LOTEM transients at early times can be reached by considering the interpretation of NanoTEM measurements (Koch, 2003). NanoTEM is a loop-loop transient electromagnetic method (Nabighian and Macnae, 1991). The maximum diffusion depth of the NanoTEM measurements at Mount Merapi was about 300 m at a total recording time of 1 ms. In fact the resistivity model of the upper 300 m derived by Koch (2003) not only resolves the resistivity structure at these shallower depths, but also constrains the position of the fault to a narrow zone around 5000 m distance from the 2001 LOTEM transmitter position. A 3D resistivity model brought forward by Müller (2000) to explain magnetotelluric induction arrows measured along a north south profile confirms the existence of an anomalous resistivity distribution in this region but does not deliver any further constrains on the position of the fault.
Stations not influenced by the presence of the fault should give insight into the deeper resistivity structure. Tests with several pairs of 1D/2D models were conducted where each 2D model contains the rough features already known and the corresponding 1D model assumes a layering equivalent to that of the southern part of the 2D model. The comparison of the forward responses leads to the conclusion that the four southern most stations from 2001 display no multi-dimensional effects if the fault is located about 5000 m away from the transmitter. Figure 5 shows the forward responses at selected stations for the 2D model shown in Figure 4 and its corresponding 1D model.
Therefore, an improved model for the resistivity structure south of the fault can then be derived from a joint inversion of the four most southern $\dot{B}_z$-components. The joint inversion was performed with Marquardt's method on a set of seven layers. The upper two layers were chosen according to the NanoTEM results and were kept fixed during the inversion. So there was a total of nine variables (five layer resistivities and four layer thicknesses). The result of this Marquardt inversion is depicted in Figure 6.
In order to keep our 2D model simple, the resistivity distribution north of the fault below 300 m depth was chosen similar to that south of the fault with the only difference that the thickness of third layer has been in-

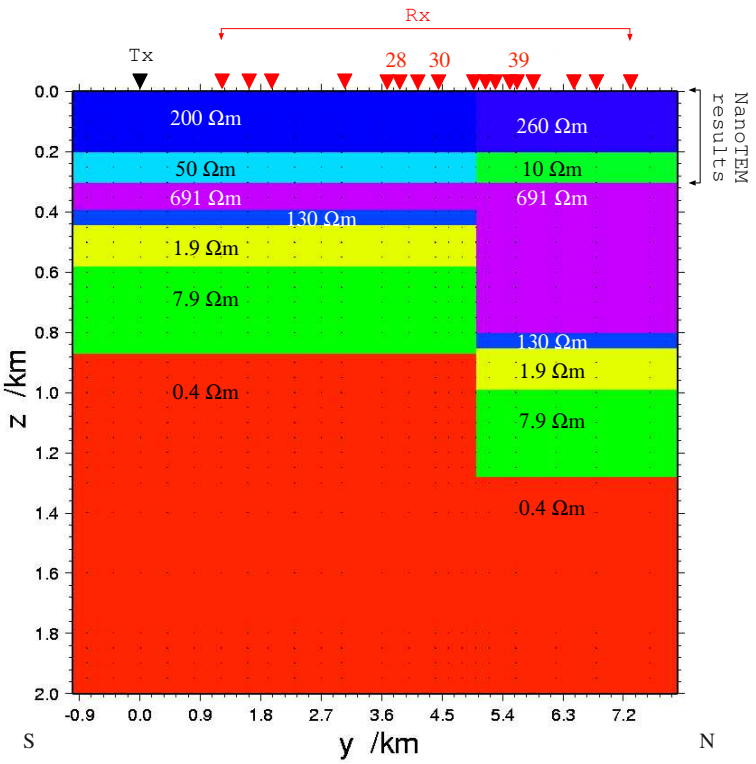

Figure 4: *The final resistivity model for the $\dot{B}_z$-transients measured in 2001 with seven layers, which are displaced to greater depth at a distance of 5000 m from the transmitter position. The uppermost layers are taken from the NanoTEM results of Koch (2003). The parameters of the remaining layers are derived by a 1D-Marquardt inversion of the $\dot{B}_z$-transients of the four southernly stations.*

creased to 500 m. The layering above 300 m depth was again chosen according to the NanoTEM results.
Our final model gives a very good data fit not only for the transients measured at the four southernly stations but also for stations on the southern section that show a stronger anomalous influence and for stations north of the supposed fault. The $\dot{B}_z$-component of station 28 (Figure 7(a)) shows a very good data fit except at very early times. Station 30 is located about 500 m south of the assumed fault (Figure 4) and shows a strong influence of the fault at about 10 ms (Figure 7(b)). The transient measured in the field is very well fitted by the model forward transient. Station 39 is one of nine stations that was recorded with the VibroTEM-method which is an adoption of the VibroSeis concept to TEM (Helwig, 2000). This method was used in parts of the measurement area with strong anthropogenic noise. VibroTEM transients are approximately the derivatives of the corresponding LOTEM-transients with respect to time. The sample transient presented in Figure 7(c) is well fitted by the forward data up to about 30 ms, where it drops below the noise level. Further 2D-forward calculations with the final model (Figure 4) for the $\dot{B}_y$-transients show a good fit between measured transients and forward responses.
Our model (Figure 4) does not allow the interpretation of the double sign changes in the $\dot{B}_z$-transients recorded during the 1998 field campaign, though. The extension of the good conductor to the surface in a dyke-shaped structure along the fault generates a few of the sign reversals observed at stations close to the assumed fault. However, as this model improves the data fit to the 1998 data it deteriorates the fit to the 2001 data. A model that reflects double sign changes at all stations to the south of the 1998 transmitter position and shows a transition to a good conductor at depth as demanded by the 2001 data could not be found yet.

5. Discussion

Although a common model for the 1998 and 2001 LOTEM/VibroTEM data sets was not found, the existence of an anomalous resistivity distribution as assumed by Müller et al. (2002) and its approximate position is confirmed by the 2001 LOTEM/VibroTEM data and by other methods. The implementation of NanoTEM results into the 2D-forward models yields an important improvement to the data fit.
A possible interpretation of high resistivities in the upper layers is a sequence of unsaturated pyroclastic layers consisting of lapilli and ash deposits with intermittent effusive layers. The existence of this layer-

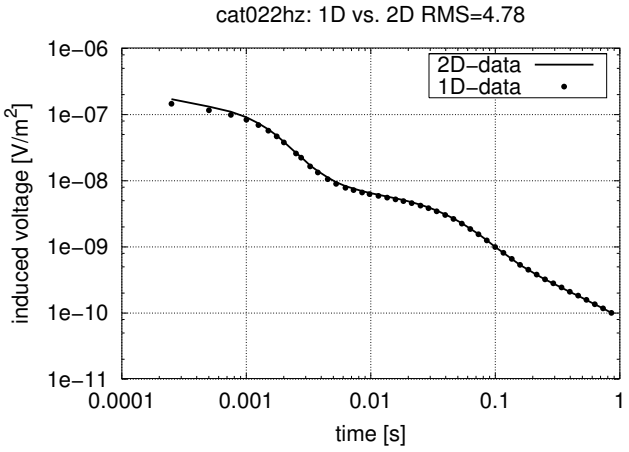

(a) $\dot{B}_z$-component of station 22

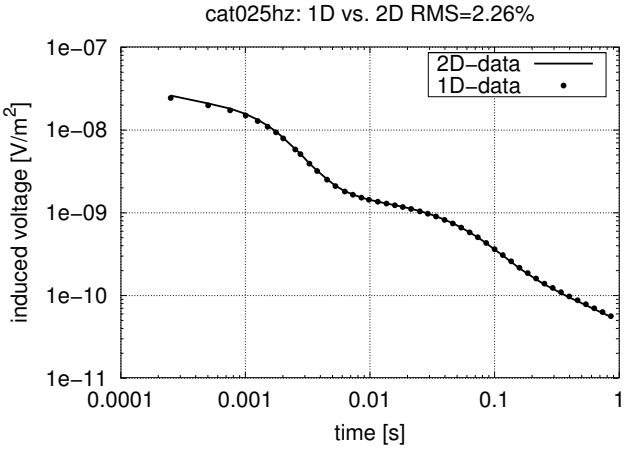

(b) $\dot{B}_z$-component of station 25

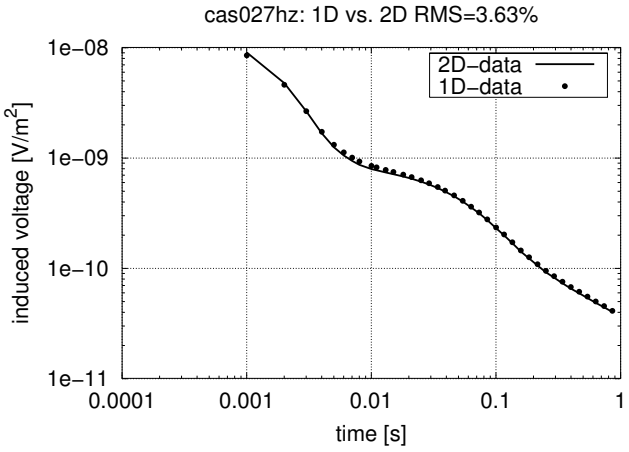

(c) $\dot{B}_z$-component of station 27

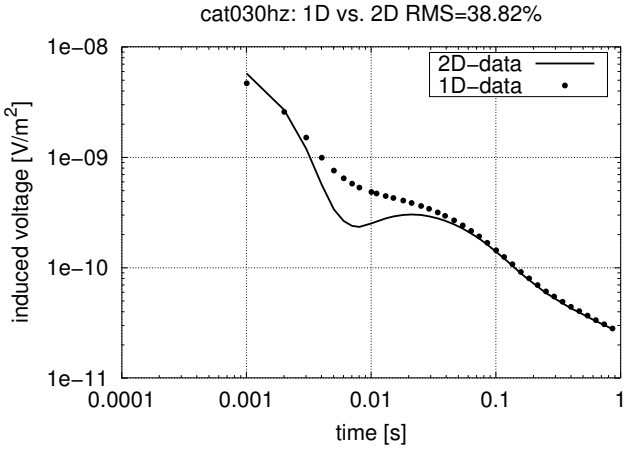

(d) $\dot{B}_z$-component of station 30

Figure 5: *Comparison of 2D-forward data of the model with seven layers and a fault from figure 4 and 1D forward data of the southern 1D-layering. The forward transients are not convolved with the system response. Stations 22 and 25 show no multidimensional effects while the transient of station 27 is slightly distorted by the fault at about 10 ms. The transient of station 30 is severely distorted.*

ing was confirmed by Gertisser and Keller (1998) for the volcanic deposits of the past 12,000 years. Merapi's total age is about 40,000 years (Camus et al., 2000). Friedel et al. (2000) attributed resistivity values of about 100 Ωm to a zone saturated by meteoric groundwater. Good conductors with resistivities below 50 Ωm were stated to arise through meteoric water that interacts with and therefore extends the hydrothermal zone closer to the summit.

Several explanations have been discussed for the resistivities below 2 Ωm of the deeper structures. A magma deposit that extends under a great area below the volcano is unlikely to cause such low resistivity values as it clearly should show up in continuous deformation monitoring experiments (Westerhaus et al., 1998). MT results along a 150 km profile across Java show a good conductor at depths of 1 - 3 km (Ritter et al., 1998) and Müller et al. (2002) proposed the conductive layer observed at mount Merapi to be a part of this regional layer across Java. Ritter et al. (1998) discussed saline fluids as the main source of the high conductivities.

We try to explain the resistivities of the good conductor below 2 Ωm with Archie's law:

$$\rho_e = a\phi^{-m}S^{-n}\rho_{fl} \tag{4}$$

where a is a proportionality factor, ϕ is the porosity, m is the cementation exponent, S describes the saturation, $n \approx 2$ is a saturation exponent and ρ_{fl} is the resistivity of the pore fluid. If we assume that the good conductor is below ground water level, all pores con-

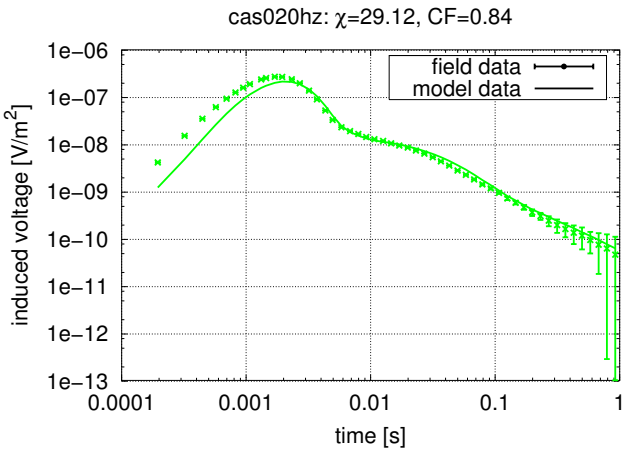

(a) $\dot{B}_z$-component of station 20

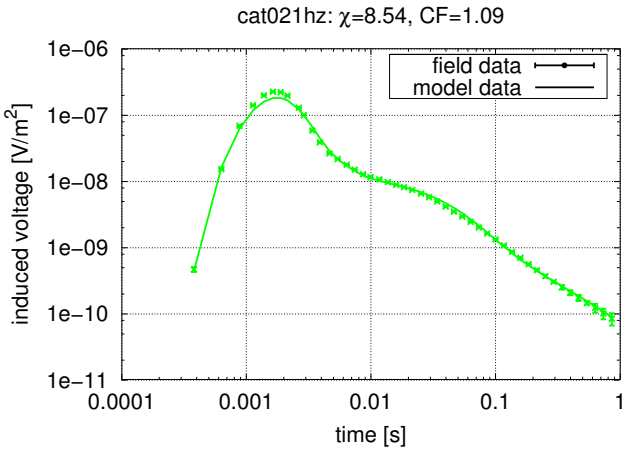

(b) $\dot{B}_z$-component of station 21

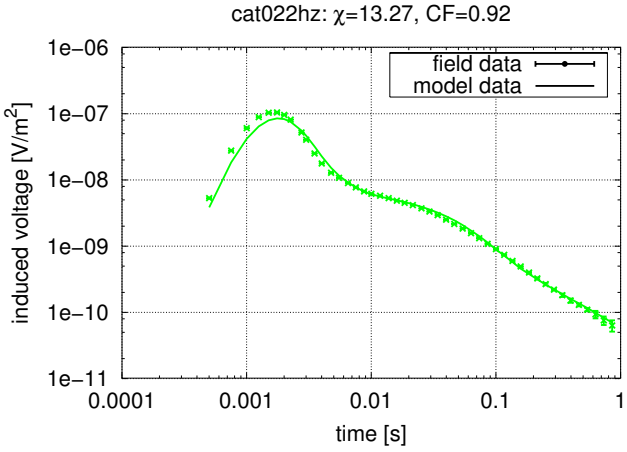

(c) $\dot{B}_z$-component of station 22

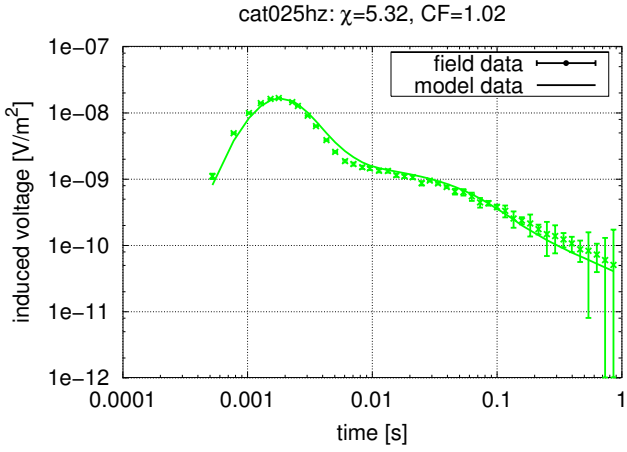

(d) $\dot{B}_z$-component of station 25

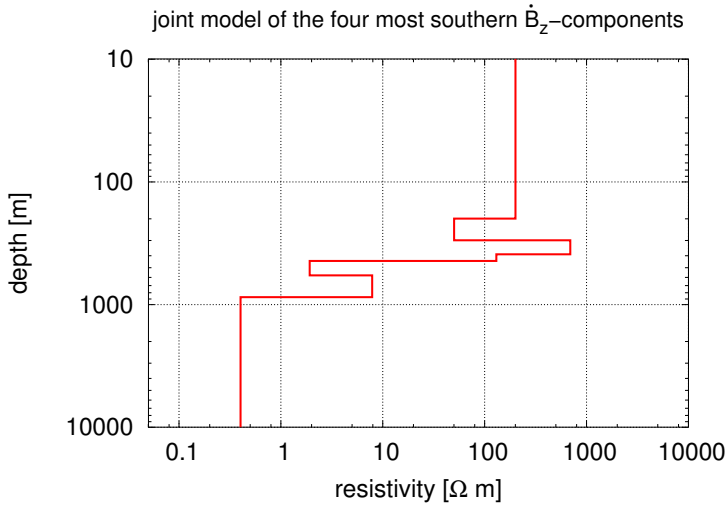

(e) Common model

Figure 6: *Results of the 1D-Marquardt inversion for the $\dot{B}_z$-components of the four southernly stations. The joint model delivers a very good fit to each transient except for early times with calibration factors (CF) close to 1.0.*

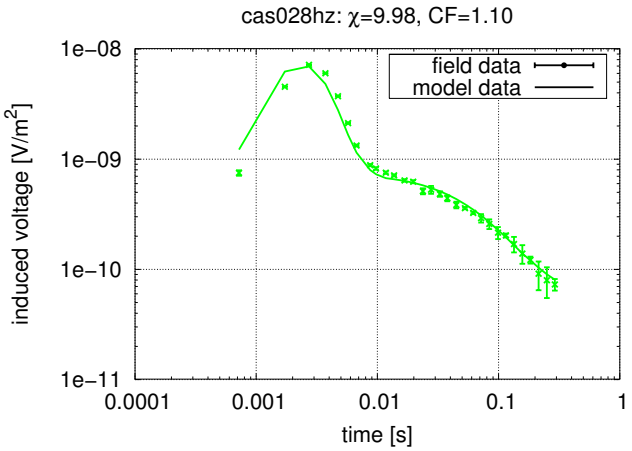

(a) $\dot{B}_z$-component of station 28

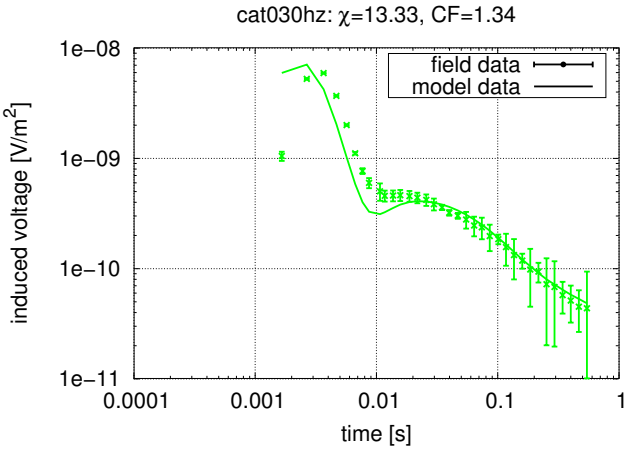

(b) $\dot{B}_z$-component of station 30

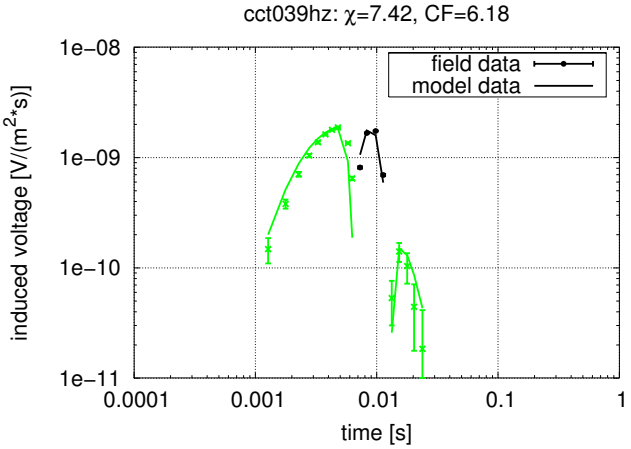

(c) $\ddot{B}_z$-component of station 39

Figure 7: *Data fit of the model forward responses of the model depicted in figure 4 to the $\dot{B}_z$-components of stations 28 and 30 and to the $\ddot{B}_z$-component of station 39.*

tain fluid ($S = 1$). Angeheister (1982) proposed porosity values up to 15 % to be realistic for volcanic sediments. According to Keller (1982) $m = 2$ is a good estimate for volcanic rocks. Hence

$$\rho_e = a0.15^{-2}\rho_{fl}\,. \tag{5}$$

Nesbitt (1993) studied the electrical resistivities of crustal fluids, in which the dissolved salt is potassium chloride (KCl). He pointed out that the conductivity properties of potassium chloride solutions are very similar to those of the more abundant sodium chloride (NaCl) solutions. At a typical crustal temperature gradient of 30 °C/km, the electrical resistivity of a KCl solution with a concentration of KCl between 3.8 wt % to 24.7 wt % should range from about 0.1 Ωm to 0.02 Ωm for a depth of about 1 km.
For $a = 1$ the rock resistivity ranges from $\rho_e = 4\,\Omega$m for $\rho_{fl} = 0.1\,\Omega$m to $\rho_e = 0.8\,\Omega$m for $\rho_{fl} = 0.02\,\Omega$m. It should be noted that these resistivity estimations may be slightly too high since a temperature gradient of 30 °C/km might be exceeded in the vicinity of a volcano.
Müller et al. (2002) brought forward another hypothesis of the highly conductive layer being locally connected with an ancient caldera event (Camus et al., 2000). Normally, hydrothermally altered minerals only exist in a zone close to the central conduit of a volcano, where the temperature ranges from 80 °C to 300 °C (Lénat, 1995). In the case of a caldera event hydrothermally altered minerals (zeolithes and clay minerals) might be present below the south flank at some distance from the current hydrothermal zone.
We propose either highly saline fluids or a combination of highly saline fluids and hydrothermally altered minerals from an ancient caldera to be responsible for the low resistivities of 0.4 Ωm observed at depths below 1 km (Figure 4).
In our model (Figure 4) we explain the multidimensional effects observed in the 2001 LOTEM/VibroTEM data with a fault at a distance of 7 km south of Merapi's summit (which corresponds to a distance of 5 km north of the 2001 transmitter position). Unfortunately, the data quality at the stations in the vicinity of the proposed fault is low. So the exact shape of the fault cannot be quantitized. On a geological map of the major tectonic surface structures of Merapi volcano, Camus et al. (2000) marked an ancient hyperbolic fault structure, which was proposed earlier by van Bemmelen (1949). The fault runs from the west of the summit around the summit and then extends to the south west of the summit. Our LOTEM profile is crossed at a distance of about 3 km south of the summit. The hyperbolic fault is interpreted as a scar of a gravitational collapse that destabilized the west-south-west flank of Merapi. The collapse triggered a violent explosive event (Camus et al., 2000). The position where the corresponding avalanche caldera rim crosses our LOTEM profile is restricted to a distance of more than 3 km south of the summit.
Camus et al. (2000) discuss the existence of "megablocks" as indicators for the extension of the avalanche caldera on Merapi's south flank. Megablocks are complex blocks of lava flows which collapsed into the avalanche caldera after the main event (Camus et al., 2000). There is contradictory geological information on the origin of the Plawangan and Turgo hills south of Merapi's summit. Both are discussed to be megablocks. The southern rims of the Plawangan and Turgo hills are at a distance of 6 km south of Merapi's summit. Consequently, if these two hills are true megablocks, it is possible that the avalanche caldera rim extends to a distance of 7 km from Merapi's summit. The fault that we have in our 2D model (Figure 4) could then coincide with the avalanche caldera rim.

References

Angeheister, G., 1982, Physical properties of rocks *in* Hellwege, K.-H., Ed., Landolt-Börnstein: Numerical Data and Functional Relationships in Science and Technology: Springer, 239–307.

Camus, G., Gourgaud, A., and Mossand-Berthommier, P.-C., 2000, Merapi (Central Java, Indonesia): An outline of the structural and magmatological evolution, with a special emphasis to the major pyroclastic events: J. Volc. Geother. Res., **100**, 139–163.

Commer, M., 1999, Ein spezielles Verfahren der eindimensionalen kombinierten Inversion von Long–Offset Transient Electromagnetic (LOTEM) – und Magnetotellurik (MT) – Daten: Master's thesis, Univ. zu Köln, Inst. für Geophys. und Meteo.

Commer, M., 2003, Three-dimensional inversion of transient electromagnetic data: A comparative study: Ph.D. thesis, Univ. zu Köln, Inst. für Geophys. und Meteo.

Constable, S. C., Parker, R. L., and Constable, C. G., 1987, Occam's inversion: A practical algorithm for generating smooth models from electromagnetic sounding data: Geophysics, **52**, 289–300.

Druskin, V. L., and Knizhnerman, L. A., 1988, Spectral differential-difference method for numeric solution of three-dimensional nonstationary problems of electric prospecting: Izvestiya: Earth Physics, **24**, 641–648.

Friedel, S., Brunner, I., Jacobs, F., and Rücker, C., 2000, New results from DC Resistivity Imaging along the flanks of Merapi Volcano *in* Zschau, J., and Westerhaus, M., Eds., Decade-Volcanoes under Investigation: Dt. Geophys. Gesellschaft, 23–29.

Gertisser, R., and Keller, J., 1998, The holocene volcanic activity and magmatic evolution of Merapi volcano , Central Java: Constraints from stratigrafic, chronologic and geochemical data *in* Zschau, J., and Westerhaus, M., Eds., Decade-Volcanoes under Investigation: Dt. Geophys. Gesellschaft, 13–14.

Helwig, S. L., 2000, VIBROTEM: Ph.D. thesis, Univ. zu Köln, Inst. für Geophys. und Meteo.

Hördt, A., 1989, Ein Verfahren zur 'Joint Inversion' angewandt auf 'Long Offset Electromagnetics' (LOTEM) und Magnetotellurik (MT): Master's thesis, Univ. zu Köln, Inst. für Geophys. und Meteo.

Keller, G. V., 1982, Electrical properties of rocks and minerals *in* Carmichael, R., Ed., Handbook of Physical properties of rocks: CRC-Press, 217–293.

Koch, O., 2003, Transient-elektromagnetische Messungen zur Erkundung einer Leitfähigkeitsanomalie am Vulkan Merapi in Indonesien: Master's thesis, Univ. zu Köln, Inst. für Geophys. und Meteo.

Lénat, J. F., 1995, Geoelectrical methods in volcano monitoring *in* McGuire, B., Kilburn, C., and Murray, J., Eds., Monitoring active volcanoes: UCL Press, 248–274.

Müller, M., Hördt, A., and Neubauer, F. M., 2002, Internal structure of Mount Merapi, Indonesia, derived from long–offset transient electromagnetic data: J. Geophys. Res., **107**, ECV2–1–ECV2–14.

Müller, A., 2000, Identification of good electric conductors below Merapi Volcano (Central Java) by magnetotellurics: DGG–Mitteilungen, Sonderband.

Nabighian, M. N., and Macnae, J. C., 1991, Time Domain Electromagnetic Prospecting Methods *in* Nabighian, M. N., Ed., Electromagnetic Methods in Applied Geophysics: Soc. Expl. Geophys.

Nesbitt, B. E., 1993, Electrical resistivities of crustal fluids: J. Geophys. Res., **98**, no. B3, 4301–4310.

Ritter, O., Hoffman-Rothe, A., Müller, A., Dwipa, S., Arsadi, E., Mahfi, A., Nurnusanto, I., Byrdina, S., Echternacht, F., and Haak, V., 1998, A magnetoteluric profile across central java, indonesia: Geophys. Res. Lett., **25**, no. 23, 4265–4268.

Spies, B. R., 1989, Depth of investigation in electromagnetic sounding methods: Geophysics, **54**, 872–888.

Strack, K. M., 1992, Exploration with Deep Transient Electromagnetics:, Methods in Geochemistry and Geophysics, Bd. 30 Elsevier, Amsterdam.

van Bemmelen, R. W., 1949, The geology of Indonesia:, volume 1A Government Printing Office, The Hague.

Vozoff, K., and Jupp, D. L. B., 1975, Joint Inversion of Geophysical Data: Geophys. J. R. astr. Soc., **42**, 977–991.

Westerhaus, M., Rebscher, D., Welle, W., Pfaff, A., Körner, A., and Nandaka, M., 1998, Deformation measurements at the flanks of Merapi Volcano *in* Zschau, J., and Westerhaus, M., Eds., Decade-Volcanoes under Investigation: Dt. Geophys. Gesellschaft, 93–100.

Zschau, J., Sukhyar, R., Purbawinata, M. A., Lühr, B., and Westerhaus, M., 1998, Project MERAPI — Interdisciplinary Research at a High-Risk Volcano Project MERAPI — Interdisciplinary Research at a High-Risk Volcano, Dt. Geophys. Gesellschaft, Decade-Volcanoes under Investigation, 3–8.